Multispectral detection of organic residues on poultry processing plant equipment based on hyperspectral reflectance imaging technique[☆]

Byoung-Kwan Cho [1], Yud-Ren Chen [*], Moon S. Kim

Instrumentation and Sensing Laboratory, U.S. Department of Agriculture, Agricultural Research Service,
Henry A. Wallace Beltsville Agricultural Research Center, Building 303, BARC-East,
10300 Baltimore Avenue, Beltsville, MD 20705, USA

Abstract

Diluted organic residues, such as feces, ingesta and other biological substances on poultry processing plant equipment surfaces, not easily discernible by human eye, are potential contamination sources for poultry carcasses. Development of sensitive detection methods for diluted organic residues is essential to ensure safe production of poultry carcasses. Hyperspectral imaging techniques have shown good potential for detecting the presence of fecal and other biological contaminants on food and processing equipment surfaces. In this study, the use of high spatial resolution hyperspectral reflectance is presented as a tool for selecting a few multispectral bands to detect diluted organic residues on the surface of materials used for manufacturing processing equipment. Reflectance imaging methods were explored for use in the detection of a range of diluted organic residues for both wet and dry conditions. Results showed that low concentrations of wet and dry residues, diluted up to 1:100 by weight with double distilled water, could be differentiated from stainless steel background with accuracies of 94.0 and 99.7%, respectively. Spectral bands determined in this study could be used for developing a multispectral inspection system for sanitation monitoring of poultry processing plants.
© 2007 Elsevier B.V. All rights reserved.

Keywords: Hyperspectral; Multispectral; Reflectance image; Fecal contamination

1. Introduction

The importance of safe and secure production of food commodities has been increasingly recognized in the current mass production environment of the meat industry. Food-related illnesses are mainly caused by bacteria, which are often transmitted through fecal matter and ingesta on meat and poultry (FSIS, 2004; FDA, 2001). Undercooked or mishandled meat and poultry carrying pathogens such as *E. coli* O 157:H7, salmonella, and listeria can cause serious human illness and even death (Cody et al., 1999; Mead et al., 1999). Inspection regulations of the United States

---

Department of Agriculture (USDA), Food Safety and Inspection Service (FSIS), require that unwholesome poultry products, which may be contaminated with human pathogens, be removed from processing lines.

During poultry processing operations, bird carcasses and processing equipment can be contaminated with ingesta from the stomach (proventriculus/gizzard), and with feces from the intestines, through incidental ruptures of the digestive tract. These contaminants may contain human pathogens and can cause cross-contamination of subsequent carcasses on the processing line. Research efforts have been made to develop optical sensing technologies that can detect fecal and ingesta residues on poultry carcasses (Park et al., 2002, 2005). However, sanitation monitoring for equipment surfaces during and after processing is also needed to reduce cross-contamination to comply with zero tolerance of contaminant free production. Diluted fecal and ingesta residues on processing equipment, in either wet or dry conditions and not easily discernable from water and background by human eye, pose contamination risks for poultry carcasses. Hence, the development of sensitive detection methods for fecal and ingesta residues is essential to ensure the safe processing of wholesome poultry products.

Recently, hyperspectral imaging techniques have been found useful for food safety applications such as the determination of a few key spectral bands for multispectral detection of contamination on food surfaces. The processing times typically needed for the large volumes of data acquired by hyperspectral imaging make its use impractical for real-time inspection at food processing plants. However, research has shown multispectral imaging to be well suited for such inspection operations, including multiple studies by USDA Agricultural Research Service (ARS) laboratories. Detection methods for fecal and ingesta contamination on poultry carcasses using visible (Vis) and near-infrared (NIR) multispectral reflectance imaging techniques derived from hyperspectral imaging studies were studied by researchers at the ARS Russell Research Center in Athens, Georgia. Results indicated that using band ratios of images at 565 and 517 nm, fecal and ingesta matter could be discriminated from poultry carcasses with approximately 92.5% accuracy (Park et al., 2002, 2005). The ARS Instrumentation and Sensing Laboratory (ISL) in Beltsville, Maryland, successfully demonstrated the detection of cattle feces on apples using hyperspectral fluorescence imaging (Kim et al., 2002). ISL researchers showed that multispectral imaging using two to four fluorescence emission bands was sufficient to detect feces on apples.

In this study, hyperspectral imaging is used to investigate the feasibility of multispectral reflectance imaging techniques for the detection of diluted poultry residues, specifically feces and ingesta, and other product residues, such as blood, skin, meat, fat, and smeared fluids from poultry skin, on poultry processing equipment surfaces. The contaminants on equipment surfaces may be found in either wet or dry conditions, contingent upon the length of time elapsed between cessation of operations and sanitation inspection, such as short breaks within a shift or overnight plant shut downs. The objective of this study was to determine the optimal wavebands and classification algorithms to detect and discriminate between diluted residues in wet and dry conditions on the surface of poultry processing equipment. Findings in this study can potentially be used for developing low-cost and wearable/portable multispectral imaging devices for sanitation monitoring of processing equipment in poultry processing plants.

2. Materials and methods

2.1. Materials

Fecal and ingesta samples were obtained from the digestive tracts of approximately 40 fresh chicken carcasses at a chicken processing plant in Cordova, Maryland, from June to November 2005. Single samples of skin, meat, and fat were extracted from each of 24 chicken carcasses. Blood samples were also collected from 24 chickens. The samples were placed in plastic bags, covered with ice, and transported to the ISL facility within 2 h. For this study, essential control variables affecting the composition of fecal and ingesta samples are listed in Table 1.

Fecal matter from the colon, ceca, small intestine, and duodenum, and ingesta from the proventriculus and gizzard, were collected in plastic containers. The dry matter content was measured to be $274.0 \pm 56 \, \mu g/g$ wet base for ingesta, and to be 149.0 ± 18, 161.0 ± 21, and $180.0 \pm 21 \, \mu g/g$ wet base, for feces from the duodenum, small intestine, and ceca, respectively. Note that the dry matter content for fecal matter from the colon was not obtained due to insufficient sample quantity. Each fecal and ingesta sample was diluted 1:5, 1:10, 1:50, and 1:100 by weight with double distilled (DD) water. Using a pipette with approximately 2 mm of the tip removed to accommodate particulates, 50 μl drops of undiluted and diluted fecal matter, ingesta, and DD water were then applied to the surface of stainless steel sheets (S30200, Allegheny Ludlum, Pittsburgh, PA, USA) commonly used for manufacturing poultry processing equipment.

Table 1
Control variables and corresponding fixed values for the experiments

Control variables	Values
Bird	7 week male and female
Diet	Soybean meal
Feed withdrawal	10 h
Water withdrawal	10 h

Blood samples were also applied in 50 µl drops. Approximately 8 mm diameter pieces of skin, meat, and fat were cut from poultry carcasses using a scalpel and gently placed on the stainless steel plate. Smeared spots were made by smearing a piece of poultry skin on the surface of the stainless steel plate. The sample residues which did not originate from within the digestive tract, i.e. the poultry blood, skin, meat, fat, and smeared organic fluid were named "product residues" to differentiate from the contaminant residues, i.e. fecal matter and ingesta. After collecting initial hyperspectral images of the steel plates with freshly applied (wet) sample residues, the samples were allowed to air dry at room temperature in the laboratory for a minimum of 24 h, after which images were acquired of the steel plates with the dried sample residues.

2.2. Hyperspectral imaging system

A schematic diagram of the ISL hyperspectral imaging system is shown in Fig. 1. It consists of a 16-bit digital imager, a spectrograph, and a lens along with a sample transport mechanism and lighting sources. The digital imager contains a thermo-electrically cooled (three-stage Peltier device), electron multiplying charge-coupled device (EMCCD) with 288 (V) × 560 (H) pixels (DV465-FL, Andor Technology Limited, South Windor, CT, USA). The line-scan spectrograph (ImSpector V9, Spectral Imaging Ltd., Oulu, Finland) is based on prism-grating-prism (PGP) optics and is coupled to an f1.4 C-mount lens (Rainbow CCTV S6X11, International Space Optics, S.A., Irvine, CA, USA). The spectrograph disperses incoming radiation from each spatial location on the scan line across the spectral dimension. The sample is scanned line-by-line with spectral range in the visible to NIR from 425.7 nm to 951.2 nm with about 4.5 nm intervals (112 wavebands). Note that for this investigation, 101 wavebands spanning the region from 450 to 900 nm were used. A programmable, precision positioning table (NF90-Bislide, Velmex Inc., Bloomfield, NY, USA) moves samples transversely through the linear field of view (FOV). The use of a programmable positioning table allows geo-spatially identical sample images for reflectance measurements acquired independently. The system was designed to capture reflectance measurements for samples up to 30 cm wide. For each line scan, the positioning table was incremented by 0.5 mm. Two 21 V, 150 W halogen lamps powered by regulated DC power supplies were used as the illuminating light source for the reflectance measurements. Light from the lamps are transmitted through optical fiber-bundles that
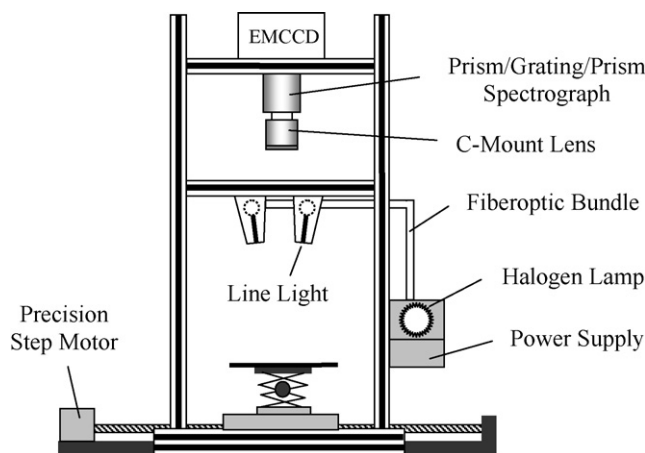

Fig. 1. Schematic illustration of the hyperspectral imaging system.

are arranged in a line (30-cm long) at the exit-end to illuminate the narrow line of the FOV. Two line lights illuminate the FOV at 5° forward and backward angles to minimize shadows caused by samples with three-dimensional features. Interface software was developed using Visual Basic (Version 6.0, Microsoft, Seattle, WA) operating in a MS Windows environment to control the EMCCD camera system and acquire image data. Individual line-scan data were saved in a 16-bit binary format along with a header file (per set) containing imaging parameter information. A white diffuse reflectance reference panel (Spectralon by Labsphere, North Sutton, NH) was used to calculate relative reflectance values (R). An R (%) for an individual pixel (i) at a given wavelength was calculated using the following equation:

$$R_i = \frac{RS_i - RD_i}{RR_i - RD_i} \times 100 \tag{1}$$

where RS, RD, and RR are the raw intensity values of an individual pixel from the sample image, dark current image, and white reference, respectively. The exposure times of the CCD and the light intensities were adjusted so that the maximum intensity level of the diffuse reference panel was approximately one third of the full dynamic range. For a detailed description of spectral and spatial calibration procedures of the ISL hyperspectral imaging system, refer to Kim et al. (2001)

2.3. Image processing

Matlab software (version 7.0.4, The Mathworks, Natick, MA) was used to process hyperspectral images and to perform analyses. To reduce the image data volume to be analyzed and to increase the signal-to-noise ratio, spatial binning of 3×3 was used. The region of interest (ROI) used for each sample residue area consisted of approximately 50 binned pixels. Spectral information of each binned pixel in the selected ROI was saved for use in determining optimal wavebands and threshold values. This study focused on selecting a single optimal waveband and also a two-waveband ratio that could be applied toward developing low-cost, portable or wearable imaging devices. Selection was based on F values of ANOVA between two groups of interest for classification, such as organic residues versus inorganic samples (stainless steel or water), or contaminant residues versus product residues. Following the waveband selection, the optimal global threshold value at which the classification accuracy was highest was determined by investigating iterative threshold increments of 0.01.

A total of over 60,000 3×3 binned pixel spectra were available. Over 10,000 of these 60,000 pixel spectra were from stainless steel surfaces. To avoid bias, equal sample sizes for individual groups were maintained. To evaluate classification accuracies for differentiating residues (including both contaminant and product residues) from stainless steel background, a data set of 45,000 randomly selected spectra was used, while for differentiating contaminant residues from product residues, a data set of 8000 randomly selected spectra was used for wet and dry conditions, respectively. For both data sets, 80% of the data was used for calibration and the remaining 20% for validation.

3. Results and discussion

3.1. Classification of wet contaminant and product residues

Preliminary evaluation of the images showed that some of the diluted samples and DD water exhibited specular responses at all wavelengths under investigation. The image on the left in Fig. 2 shows the reflectance image at 469 nm of representative ceca samples (1:5, 1:50, and 1:100 dilution) and DD water on the stainless steel plate. Fig. 2 shows that specular effects of the line lights are visible for the 1:100 freshly diluted ceca sample and for DD water. Mean reflectance spectra of the ROIs in the image are also shown in Fig. 2, including specular and non-specular regions of freshly diluted feces and DD water drop samples, and stainless steel surface. The spectra show that the relative reflectance for specular regions of the samples was higher than 100% (relative to the reflectance of the white reference panel) at all wavelengths. Even the non-shiny stainless steel surfaces showed specular reflectance characteristics, as evidenced by higher than 100% reflectance. Several factors, such as the sample geometry, illumination and sensor view angles, can also affect the observed reflectance, especially for that of the specular samples. Since the R values of diluted feces fell within the same range of R values for stainless steel, specular ceca and water, and water at the boundary region, it was difficult to discriminate the diluted fecal matter using a single waveband.
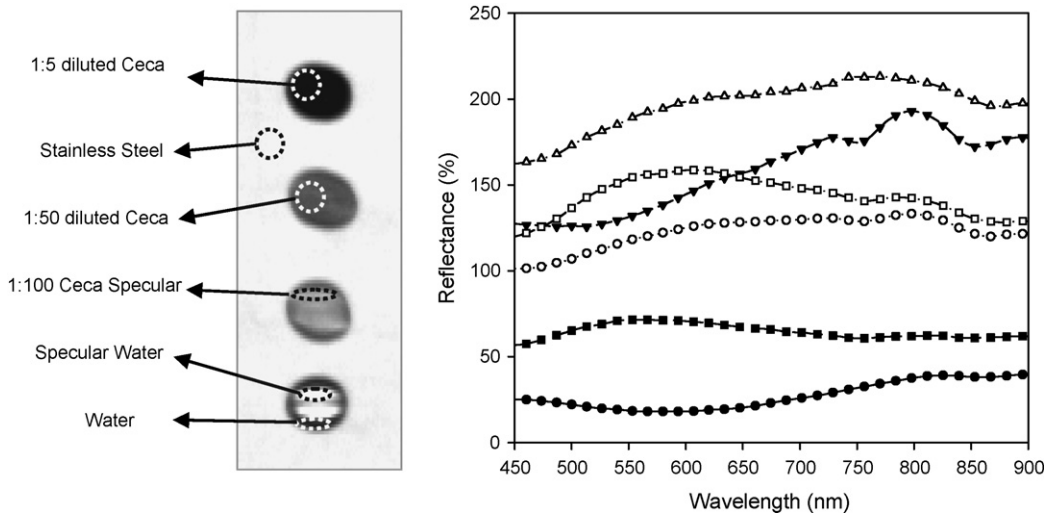
Fig. 2. Representative mean spectra of 1:5 (●) and 1:50 diluted (○) non-specular and specular regions of 1:100 diluted ceca (▼), specular (△) and edge region (■) of DD water drop, and stainless steel surface (□).

Fig. 3a shows representative spectra of undiluted feces and ingesta samples. The shapes of the spectra were similar to those of the previous study (Park et al., 2005); however, R values were relatively higher due to the light scattering from the surrounding specular background. The feces and ingesta spectra exhibited absorption features in the visible region that may be associated with the feedstuff. A study has shown that protoporphrin IX is a major constituent found in chicken feces that can affect the spectral shapes (Kim et al., 2003). In general, R values of fecal matter varied with the location within the digestive tract from which the fecal matter originated. Representative mean spectra of product residues (blood, skin, meat, fat, and skin smear) are shown in Fig. 3b. The R values of skin smear (a transparent coating) resembled the stainless steel since the incident light is minimally absorbed through the thin oily film. The spectrum of blood shows high absorption at wavelengths shorter than red. The absorption characteristics of oxymyoglobin were observed at around 545 and 580 nm (Liu et al., 2000). The above observations suggest that when using a single spectral band, detection and classification of fecal contamination may be difficult due to the transparency and specular nature of samples placed on highly reflective background surfaces.

Results based on the analyses of single R bands were not found to be useful and were omitted for brevity. F values of one-way ANOVA for the residues and background materials (stainless steel and water) were calculated for all possible
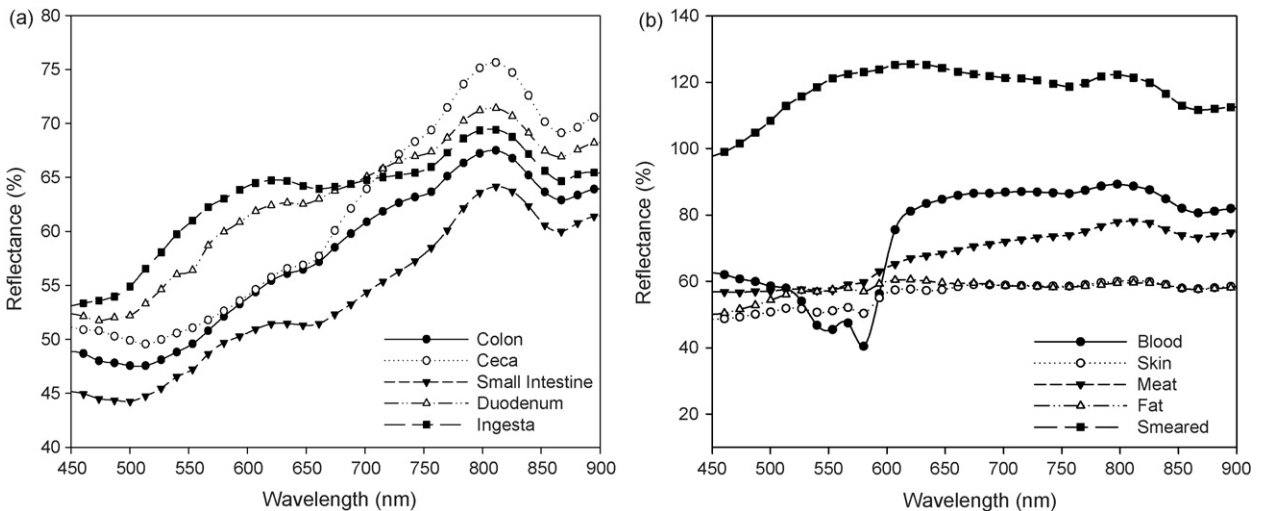

Fig. 3. Representative mean spectra of wet (a) poultry fecal and ingesta contaminant residues and (b) poultry product residues.
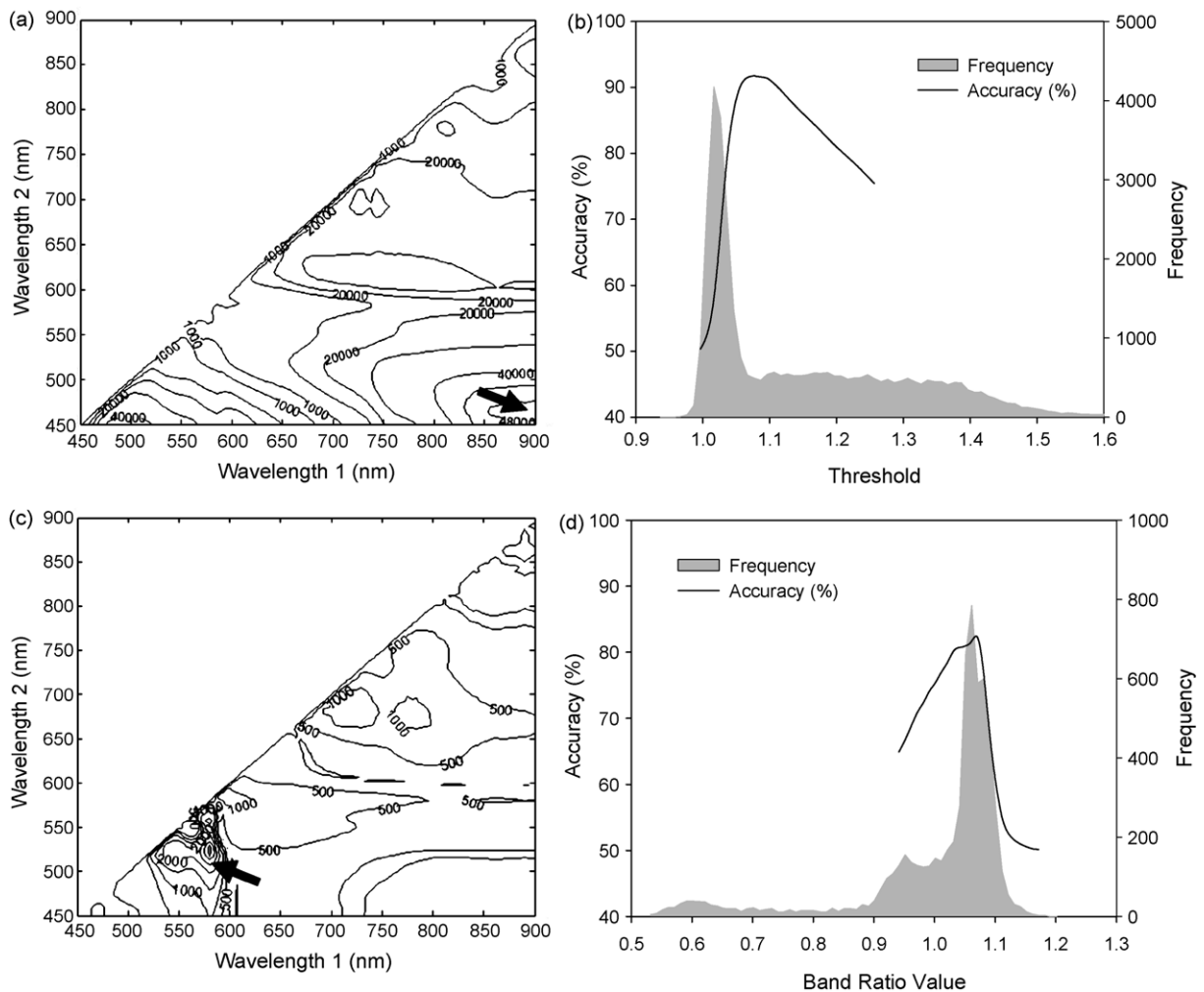
Fig. 4. Wavebands and threshold value selection. (a) *F* values for wavelength pairs used for discriminating wet residues from stainless steel and water, and (b) classification accuracy as a function of R895/R469 band ratio threshold value, with frequency histogram for ratio values of wet residues and water/stainless steel background. (c) *F* values for wavelength pairs used for discriminating wet contaminant residues from wet products residues, and (d) classification accuracy as a function of R580/R527 band ratio threshold value with frequency histogram for ratio values of wet contaminant residues and wet product residues.

two-waveband combinations in the 450–900 nm region to find the best waveband ratio pair for discriminating wet residues from the background. A larger *F* value indicates a more statistically significant mean separation between the two groups. Fig. 4a shows a contour plot of the *F* values obtained from ANOVA for the residues and background groups. The result shows that the means of the two groups were most significantly separated by a two-band ratio at 469 and 895 nm wavelengths (R895/R469). Ratio values of the residues (contaminant and product) at these two wavebands were significantly higher than those of stainless steel and water background. Classification accuracy was then calculated for each value within the range of that band ratio to find an optimal threshold value. To find an optimal threshold ratio value for separating wet residues from steel and water, classification accuracies were calculated for values across the range of ratio values. Fig. 4b shows a plot of classification accuracy as a function of R895/R469 used as the threshold for classification. Results indicated that for the R895/R469 band ratio, the highest classification accuracy (91.8%) for residues versus stainless steel and water was obtained by using a threshold value of 1.07. This observation is illustrated by the frequency histogram; although the two groups show overlap due to the large variation in ratio values for the residue groups, the relatively low ratio values, mostly from stainless steel and water samples, are largely grouped together with a peak value at 1.025 in contrast to the wider spread of a higher ratio values for the contaminant and product residues.

Table 2
Validation results of classification for wet samples

Class	Type	Dilution	Residues vs. background			Contaminant vs. product residues		
			Corr[a]	Incorr[b]	% Accuracy	Corr[a]	Incorr[b]	% Accuracy
Background	Water	–	334	533	38.5			
	Stainless steel	–	3626	7	99.8			
	Total (background)		**3960**	**540**	**88.0**			
Residues								
Contaminant residues								
	Colon	None	128	0	100	12	18	40.0
		1:5	161	0	100	12	21	36.4
		1:10	134	1	99.3	18	17	51.4
		1:50	130	5	96.3	21	7	75.0
		1:100	136	12	91.9	18	11	62.1
		Total	689	18	97.5	81	74	52.3
	Ceca	None	125	0	100	4	14	22.2
		1:5	106	5	95.5	3	19	13.6
		1:10	120	3	97.6	6	10	37.5
		1:50	120	3	97.6	12	6	66.7
		1:100	111	8	93.3	12	4	75.0
		Total	582	19	96.8	37	53	41.1
	Small intestine	None	155	0	100	22	8	73.3
		1:5	204	0	100	47	3	94.0
		1:10	204	1	99.5	37	3	92.5
		1:50	168	17	90.8	33	7	82.5
		1:100	137	33	80.6	22	15	59.5
		Total	868	51	94.5	161	36	81.7
	Duodenum	None	161	3	98.2	26	3	89.7
		1:5	192	2	99.0	41	8	83.7
		1:10	197	4	98.0	36	5	87.8
		1:50	158	23	87.3	20	14	58.8
		1:100	151	27	84.8	25	10	71.4
		Total	859	59	93.6	148	40	78.7
	Ingesta	None	177	5	97.3	20	17	54.1
		1:5	176	2	98.9	35	7	83.3
		1:10	167	13	92.8	27	8	77.1
		1:50	120	46	72.3	19	11	63.3
		1:100	92	48	65.7	10	16	38.5
		Total	732	114	86.5	111	59	65.3
	Total (contaminant residues)			–		**538**	**262**	**67.3**
Product residues								
	Blood	None	132	1	99.2	194	0	100
	Skin	–	91	2	97.8	141	0	100
	Meat	–	82	0	100	128	11	92.1
	Fat	–	81	7	92.0	157	1	99.4
	Smeared	–	113	0	100	146	22	86.9
	Total (product residues)		499	10	98.0	**766**	**34**	**95.8**
Total (residues)			**4229**	**271**	**94.0**		–	

[a] Correctly classified.
[b] Incorrectly classified.

The two-band ratio and simple threshold methods were also applied to investigate the feasibility for discriminating the fecal and ingesta contaminant residues from the product residues (blood, skin, meat, fat, and skin smear). From all the two-band combinations available, the ratio of reflectances at the wavebands at 527 and 580 nm (R580/R527) showed the highest F value from the ANOVA between the contaminant residue and product residue groups (Fig. 4c). Usually the ratio values of the feces and ingesta were higher than those of the product residues. The best classification accuracy was obtained with a threshold band ratio value of 1.07. The two wavebands, 527 and 580 nm, to discriminate contaminant residues from product residues obtained in this study were slightly different from the wavebands (e.g. 517 and 565 nm) reported by other group (Park et al., 2002, 2005). Although they differed by only 10–15 nm, the difference may emanate from variations in feedstuff and the inclusion of diluted feces and ingesta, blood, meat, and smeared organic fluid in this study.

The wavelengths and threshold values observed with the calibration data set were validated with an independent test data set. The detailed validation results are listed in Table 2 for discriminating all residues from water and the stainless steel background, and for discriminating specific contaminant residues and product residues. Against the background (stainless steel and water), the first three columns show the validation results for classification of residues as residues versus background (stainless steel or water). The classification accuracies for the feces and ingesta without dilution and diluted up to 1:5 were greater than 97.3 and 95.5%, respectively. The accuracy markedly decreased for dilutions greater than 1:50. The stainless steel was correctly classified at 99.8%; however, 61.5% of water drops were incorrectly
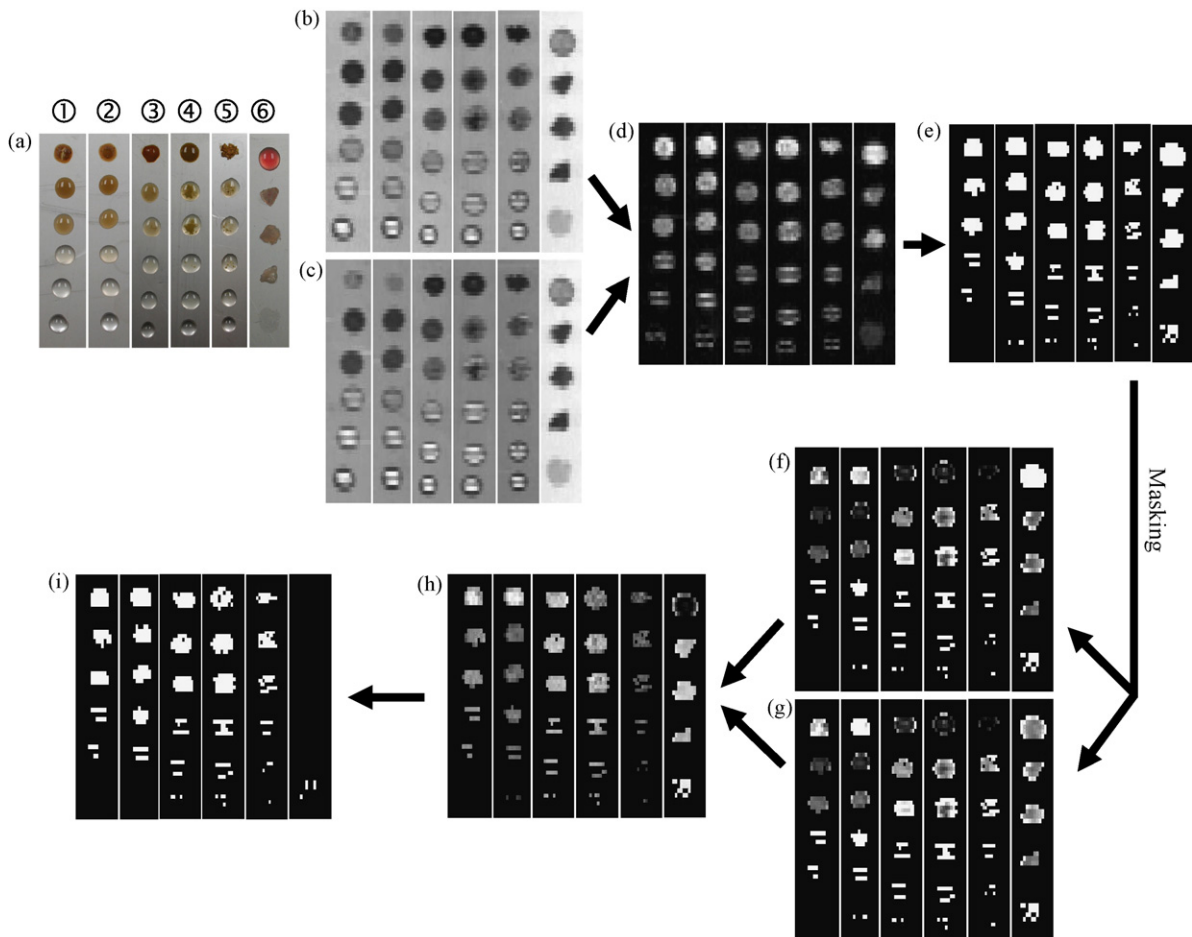

Fig. 5. (a) Photo of wet poultry contaminant and product residues on a stainless steel plate; illustration of the image processing sequence: 3 × 3 binned images (b) at 469 nm and (c) at 895 nm, (d) two-waveband ratio image (R895/R469), (e) binary image from a threshold of 1.07 applied to the ratio image, images at (f) 527 nm and (g) 580 nm after masking, (h) two-waveband ratio image (R580/R527), and (i) detection of contaminant residues using the resultant binary image from applying a threshold of 1.07 to the R580/R527 ratio image.

classified and could be significant sources of false positives. The overall validation accuracy for discriminating all residues from DD water and stainless steel was 94.0% with 12.0% of false positive.

In classifying residues as contaminant residues versus product residues, the classification accuracies for identifying product residues (the last column) were much higher than those for identifying the fecal and ingesta contaminant residues (95.8% versus 67.3%). This may be due to the much lower variation displayed by the product residue samples, compared to the contaminant residues and their wide range of dilutions.

An algorithm using images at 469 and 895 nm wavebands was developed for detecting the full range of diluted feces and ingesta on strainless steel background, inspite of the existing product residues and water drops on it. Beginning with a photo of a set of wet residue samples on a stainless steel plate, Fig. 5 shows a sequence of processed images illustrating the application of the multispectral preprocessing, two-band ratio and thresholding methods for classifying the residues. In each of the first five columns, samples are arranged from top to bottom with no dilution in row 1, with dilutions (by weight) of 1:5, 1:10, 1:50, and 1:100 in rows 2–5, and with samples of DD water in row 6 along the bottom. The contaminant materials shown in columns 1–5 (from left to right) are fecal matter from the colon, ceca, small intestine, and duodenum, and ingesta, respectively. Samples of product residues are arranged in column 6 from top to bottom as follows: blood, skin, meat, fat, and skin smear. Fig. 5b and c are 469 and 895 nm waveband images after 3×3 binning. The displayed intensity range of each column image in Fig. 5b and c was between 1 and 99% of respective maximum intensity; hence, the intensity ranges of the individual column images are not the same. Fig. 5d is a R895/R469 band ratio image, resulting from dividing the reflectance intensity at 895 nm by that at 469 nm. The water drop samples and stainless steel areas are noticeably darker than the other samples in the ratio images. Fig. 5e is the binary-classification image created from the 1.07 threshold value to the R895/R469 band ratio image. Portions of the highly diluted feces spots are missing, and parts of water drops are shown as contaminant residues (false positives). Fig. 5f and g are the 527 and 580 nm images after masking with Fig. 5e to identify residue areas. Fig. 5h is a R580/R527 band ratio image resulting from dividing the reflectance intensity at 580 nm by that at 527 nm. The resultant binary image obtained by applying a threshold of 1.07 to the R580/R527 band ratio image showed the detection of almost the full range of diluted feces and ingesta (Fig. 5i). The image also shows a few false positives for the product residues.

3.2. Classification of contaminant and products residues allowed to air dry

Fig. 6 shows representative reflectance spectra for undiluted, 1:5 and 1:50 diluted fecal matters, product residues, and stainless steel that were allowed to air dry for 24 h at room temperature. The R values of stainless steel are significantly higher than those of the contaminant and product residues throughout the entire spectral region from 450–900 nm.
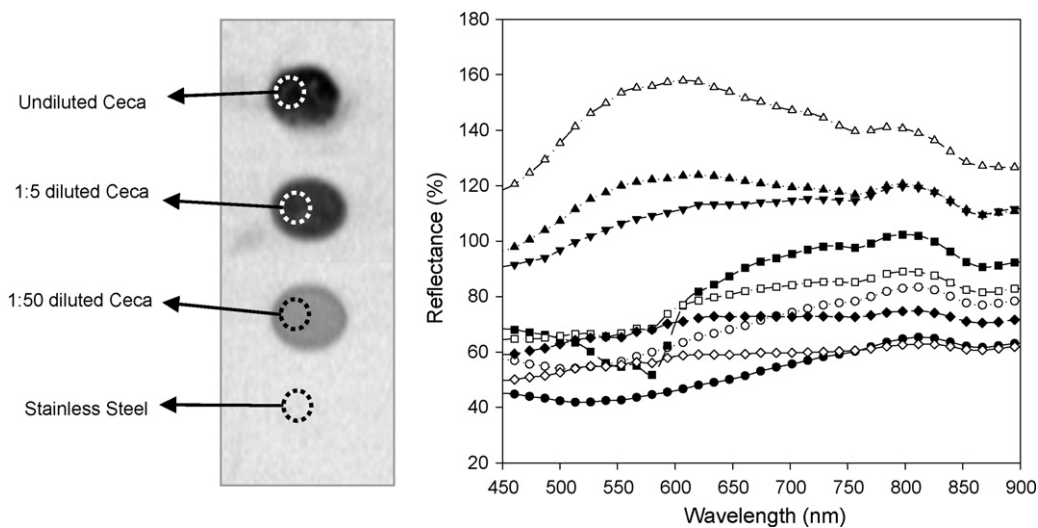

Fig. 6. Representative mean spectra of dry undiluted (●), 1:5 (○) and 1:50 diluted (▼) ceca, blood (■), skin (□), meat (◆), fat (◇), and skin smear (▲) residues and stainless steel (△).
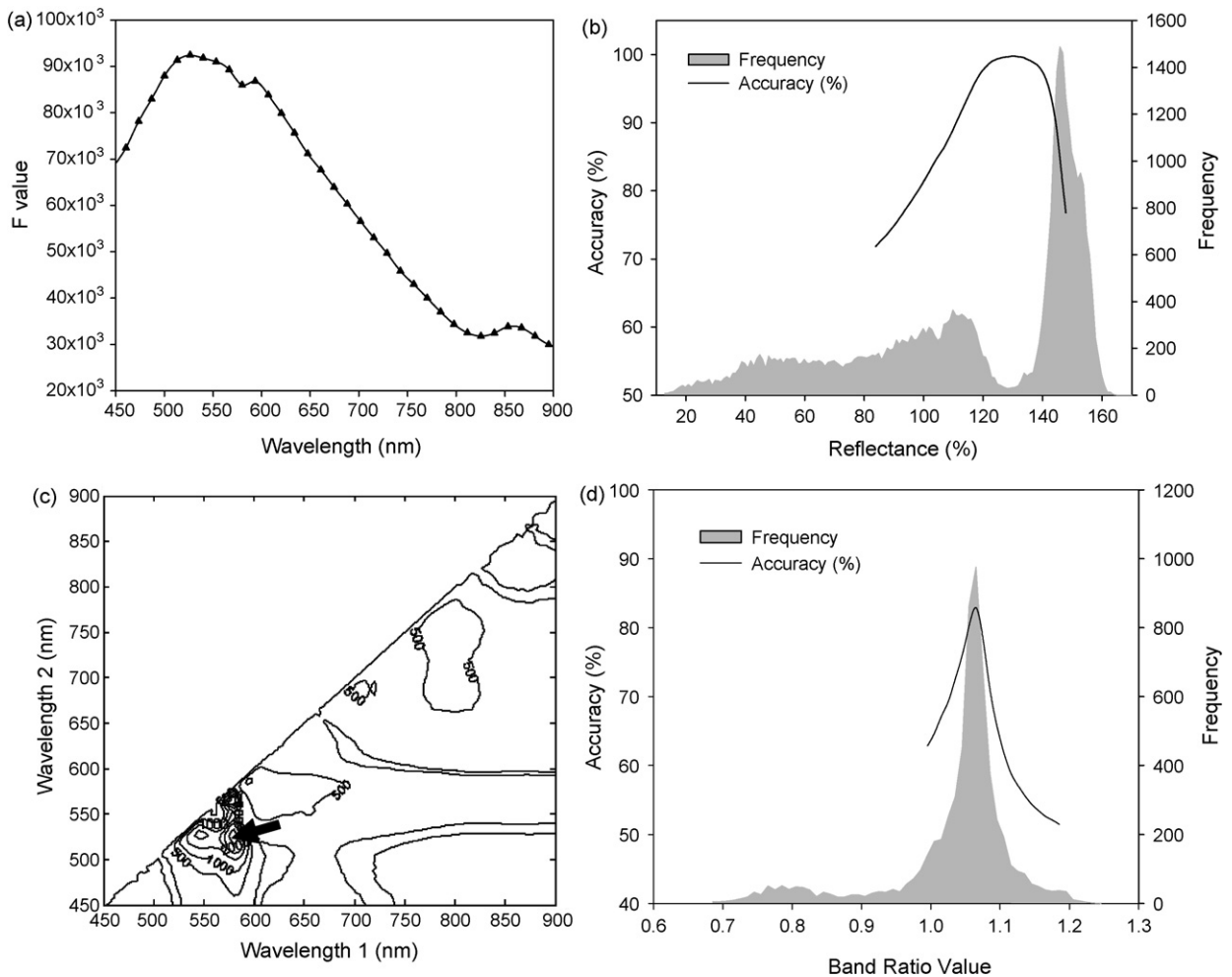
Fig. 7. Wavebands and threshold value selection. (a) *F* values by single wavelength used for discriminating dry residues from stainless steel, and (b) classification accuracy as a function of 527 nm reflectance threshold value with frequency histogram for reflectance values of dry residues and steel background. (c) *F* values for wavelength pairs used for discriminating dry contaminant residues from dry product residues, and (d) classification accuracy as a function of R580/R527 band ratio threshold value with frequency histogram for ratio values of dry contaminant residues and dry product residues.

Therefore, stainless steel can be easily discriminated with a simple threshold value. *F* values of one-way ANOVA for reflectance values of stainless steel and dry residues were calculated and are shown in Fig. 7a. The *R* values at 527 nm appeared to show the most significant differences between the two groups. Residues and stainless steel were classified with the highest accuracy (99.8%) at a threshold *R* value of 129.73%. The histogram (Fig. 7b) also exhibits distinctive distributions for the *R* values of the two groups.

Since the spectra of fecal, ingesta, and product residues cannot be accurately classified with a single waveband, the two-band ratio method used for the wet samples was also applied to the spectral data for dried residues. Fig. 7c shows *F* values of ANOVA for the ratio values of the dry contaminant and product residue samples. The highest *F* value was observed for the ratio of 580 and 527 nm, which were the same wavebands found for the wet residues. Using this same R580/R527 band ratio and a threshold value of 1.07, the dry contaminants and product residue samples were correctly classified with an accuracy of 82.9% (Fig. 7d). The validation results are listed in Table 3. The validation accuracies were 100% for discriminating dried fecal and ingesta residues diluted up to 1:50 from stainless steel. The overall classification accuracy for discriminating dried residues from stainless steel was 99.7%, with 0.2% false positives, which was better than that achieved for the wet samples. The classification accuracies for discriminating dried fecal and ingesta contaminant residues from dried product residues ranged from 29 to 100%. The

Table 3
Validation results of classification for dry samples

Class	Type		Dilution	Residues vs. background			Contaminant vs. product residues		
				Corr[a]	Incorr[b]	% Accuracy	Corr[a]	Incorr[b]	% Accuracy
Background	Stainless steel		–	**4491**	**9**	**99.8**			
Residues									
Contaminant residues									
	Colon		None	150	0	100	16	16	50.0
			1:5	157	0	100	24	1	96.0
			1:10	154	0	100	32	7	82.1
			1:50	141	0	100	15	8	65.2
			1:100	143	1	99.3	28	7	80.0
			Total	745	1	99.9	115	39	74.7
	Ceca		None	145	0	100	7	17	29.2
			1:5	137	0	100	27	4	87.1
			1:10	125	0	100	25	0	100
			1:50	114	0	100	27	0	100
			1:100	120	1	99.2	27	1	96.4
			Total	641	1	99.8	113	22	83.7
	Small intestine		None	171	0	100	27	9	75.0
			1:5	180	0	100	44	0	100
			1:10	189	0	100	46	1	97.9
			1:50	152	0	100	31	6	83.8
			1:100	141	1	99.3	19	7	73.1
			Total	833	1	99.9	167	23	87.9
	Duodenum		None	175	0	100	32	2	94.1
			1:5	175	0	100	32	0	100
			1:10	162	0	100	37	1	97.4
			1:50	143	0	100	27	4	87.1
			1:100	131	0	100	18	7	72.0
			Total	786	0	100	146	14	91.3
	Ingesta		None	174	0	100	38	10	79.2
			1:5	144	0	100	21	3	87.5
			1:10	135	0	100	16	9	64.0
			1:50	144	0	100	20	7	74.1
			1:100	130	10	92.9	23	14	62.2
			Total	727	10	98.6	118	43	73.3
	Total (contaminant residues)				–		**659**	**141**	**82.4**
Product residues									
	Blood		None	169	0	100	180	1	99.4
	Skin		–	145	0	100	134	13	91.2
	Meat		–	111	0	100	110	15	88.0
	Fat		–	168	1	99.4	154	19	89.0
	Smeared		–	161	0	100	111	63	63.8
	Total (product residues)				–		**689**	**111**	**86.1**
		Total (residues)		**4486**	**14**	**99.7**		–	

[a] Correctly classified.
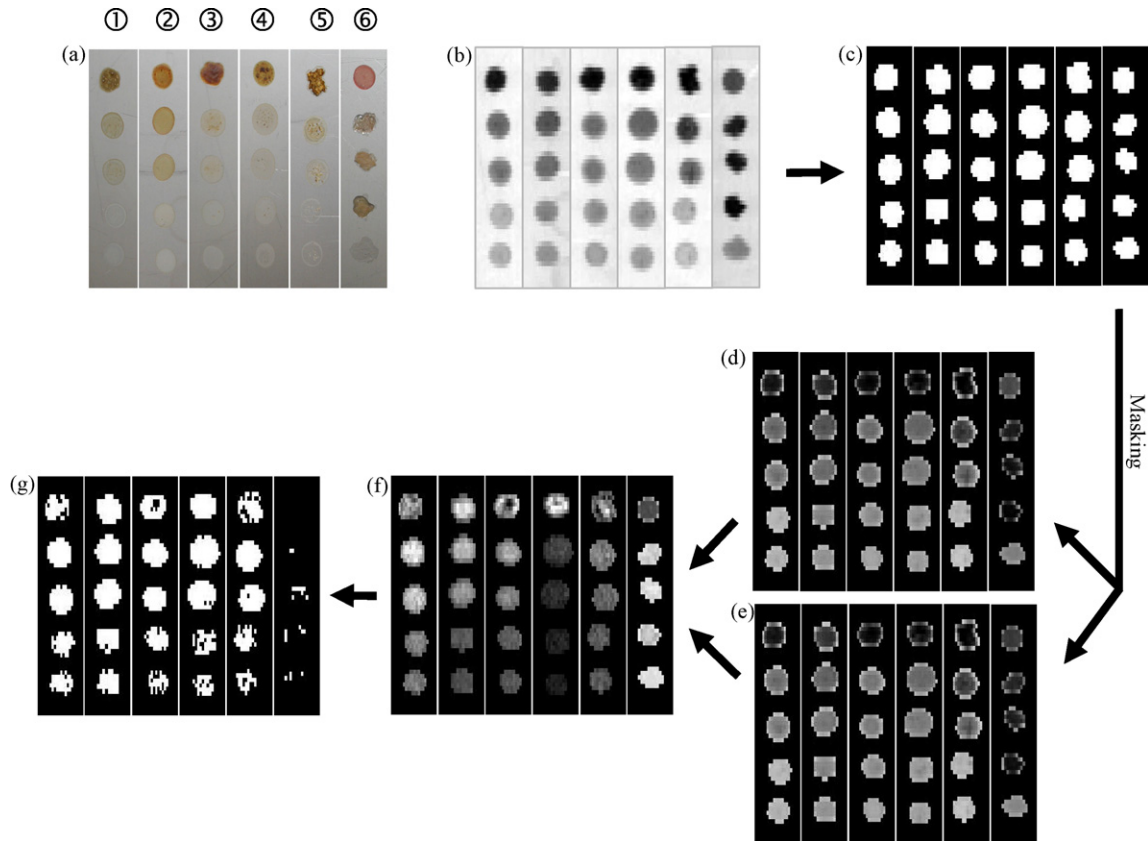[b] Incorrectly classified.

Fig. 8. (a) Photo of dried poultry contaminant and products residues on a stainless steel plate; illustration of image processing sequence: (b) 3×3 binned image at 527 nm, (c) binary image from applying a threshold of 129.73 to the 527 nm image, images at (d) 527 nm and (e) 580 nm after masking, (f) two-waveband ratio (R580/R527) image, and (g) detection of contaminant residues using the resultant binary image from applying a threshold of 1.07 to the R580/R527 image.

overall classification accuracy for discriminating dried contaminant residues from dried product residues was 82.4%, with 13.9% false positives. Although the overall classification accuracy for discriminating dried feces and ingesta from product residues was improved, the incidence of false positives also increased compared to the incidence for wet samples.

Fig. 8 shows a sequence of processed images illustrating the application of the multispectral preprocessing, two-band ratio and thresholding methods for classifying the residues. Beginning with a photo of a set of residue samples on a stainless steel plate that were allowed to air dry at room temperature for 24 h, the regions of stainless steel were eliminated from the 527 nm waveband image (Fig. 8b) using a 129.73% R value as a threshold. The resultant image (Fig. 8c) shows that most of the dried residues were successfully discriminated from the stainless steel surface. This image was used as a mask for further processing to classify dried contaminants versus dried product residues. After using the mask to remove the background steel areas on the 527 and 580 nm images (Fig. 8d and e), a two-band intensity ratio using those two waveband images was performed to discriminate the dried feces and ingesta residues from the dried product residues (Fig. 8f). The resultant binary image obtained by applying a threshold of 1.07 to the ratio image showed the detection of the range of diluted and dried fecal and ingesta matter residues (Fig. 8g). Most of the pixels in the dry blood sample area were successfully eliminated; however a few false positives were observed in the sample areas for skin, meat, fat, and skin smear residues. The dry contaminants were discriminated from the product residues using a ratio of two wavebands that included the 527 nm waveband that was also used to separate dry residues from stainless steel. Hence, only two wavebands were needed for discriminating dried contaminants, while at least four wavebands (for two different band ratios) were necessary for classifying wet contaminant residues.

4. Conclusion

The goal of this study was to investigate the feasibility of multispectral reflectance imaging technique for detection of poultry contaminant and product residues on processing equipment surfaces. A two-band reflectance image ratio using spectral bands at 469 and 895 nm (R895/R469) was capable of detecting (against background water and stainless steel) wet residues diluted up to 1:100 by weight with an accuracy of 94.0%. Another two bands at 527 and 580 nm were found to be the best for a two-band ratio (R580/R527) to discriminate wet contaminant residues from wet product residues with an accuracy of 67.3%. Dry residues could be detected (against stainless steel background) using a single waveband, 527 nm, with an accuracy of 99.7%. Fecal and ingesta contaminants which were dried in room temperature could be discriminated from dried product residues by a band ratio using the 580 and 527 nm wavebands (R580/R527), with an accuracy of 82.4%. The possible explanation for the higher classification accuracies for detecting organic residues from background water and stainless steel than those for detecting contaminant residues from product residues may be due to the distinctive reflectance spectra of inorganic materials, compared to those of the organic residues. For classification of contaminant residue and product residue samples using the two-band ratio method, the band ratio of the 580 and 527 nm wavebands (R580/R527) was found to result in the highest accuracies, regardless of wet or dried sample condition. However, results indicated that this imaging technique yielded better accuracy in detection dried residues than wet residues on processing plant equipment. The wavebands investigated in this study could be helpful for developing low cost and portable/wearable multispectral devices for monitoring the sanitation of poultry processing plants.

Acknowledgements

References

Cody, S.H., Glynn, M.K., Farrar, J.A., Cairns, K.L., Griffin, P.M., Kobayashi, J., Fyfe, M., Hoffman, R., King, A.S., Lewis, J.H., Swanminathan, B., Bryant, R.G., Vugia, D.J., 1999. An outbreak of Escherichia coli O157:H7 infection from unpasteurized commercial apple juice. Ann. Intern. Med. 130, 202–209.

Food and Drug Administration (FDA), 2001. Hazard analysis and critical control point (HAACP); Procedures for the safe and sanitary processing and importing of juices. Fed. Reg. 66, 6137–6202.

Food Safety and Inspection Service (FSIS), 2004. Livestock post-mortem inspection activities-enforcing the zero tolerances for fecal materials, ingesta, and milk. FSIS Directive 6420.2, http://www.fais.usda.gov.

Kim, M.S., Chen, Y.R., Mehl, P.M., 2001. Hyperspectral reflectance and fluorescence imaging system for food quality and safety. T. ASAE. 44, 721–729.

Kim, M.S., Lefcourt, A.M., Chen, Y., 2003. Optimal fluorescence excitation and emission bands for detection of fecal contamination. J. Food Prot. 66, 1198–1207.

Kim, M.S., Lefcourt, A.M., Chen, Y., Kim, I., Chao, K., Chan, D., 2002. Multispectral detection of fecal contamination on apples based on hyperspectral imagery - part 2: application of fluorescence imaging. T. ASAE. 45, 2039–2047.

Liu, Y., Chen, Y., Ozaki, Y., 2000. Two-dimensional visible/near-infrared correlation spectroscopy study of thermal treatment of chicken meats. J. Agric. Food Chem. 48, 901–908.

Mead, P.S., Slutsker, L., Dietz, V., McCaig, L.F., Bresee, J.S., Shapiro, C., Griffin, P.M., Tauxe, R.V., 1999. Food-related illness and death in the United States. Emerging Infectious Diseases. 5, 607–625.

Park, B., Lawrence, K.C., Windham, W.R., Buhr, R.J., 2002. Hyperspectral imaging for detection fecal and ingesta contaminations on poultry carcasses. T. ASAE. 45, 2017–2026.

Park, B., Lawrence, K.C., Windham, W.R., Smith, D.P., 2005. Detection of cecal contaminations in visceral cavity of broiler carcasses using hyperspectral imaging. Appl. Eng. Agric. 21, 627–635.